Applied Catalysis B: Environmental 89 (2009) 484–493

Contents lists available at ScienceDirect

Applied Catalysis B: Environmental

journal homepage: www.elsevier.com/locate/apcatb

# A new synthesis of a highly dispersed and CO tolerant PtSn/C electrocatalyst for low-temperature fuel cell; its electrocatalytic activity and long-term durability

Dong-Ha Lim, Dong-Hyeok Choi, Weon-Doo Lee, Ho-In Lee *

*School of Chemical and Biological Engineering and Research Center for Energy Conversion and Storage, Seoul National University, 599 Gwanangno, Gwanak-gu, Seoul 151-744, Republic of Korea*

ARTICLE INFO

*Article history:*
Received 16 July 2008
Received in revised form 30 December 2008
Accepted 17 January 2009
Available online 24 January 2009

*Keywords:*
PtSn/C electrocatalysts
Borohydride reduction and hydrothermal treatment
Methanol oxidation
CO tolerance
Long-term durability
Low-temperature fuel cell

ABSTRACT

An effective method is developed for preparing highly dispersed and nano-sized PtSn/C electrocatalysts synthesized by borohydride reduction and subsequent hydrothermal treatment. From the XRD patterns, the Pt(2 2 0) peak of the PtSn/C catalysts shift slightly to lower 2θ values with increasing Sn content, compared with that of the Pt/C catalyst, suggesting the alloy formation. Based on the HR-TEM, the PtSn nanoparticles show average particle sizes of approximately 2.3 nm on the carbon surface, which is consistent with XRD data. The XPS result shows that the slight shift in the bulk metallic Pt(0) to higher binding energies is attributed to a significant contribution from the metal-support interaction and the nano-size effect. The methanol and CO oxidations on the PtSn/C catalysts occur at lower potentials as compared to the commercial Pt/C catalyst. This result suggests that Sn has the ability to promote the oxidation of adsorbed CO at lower potentials. In the single-cell and accelerated durability tests, the 3Pt1Sn/C catalyst shows higher performance under a pure $H_2$ and CO-containing $H_2$ gases and better durability under a 0.5 M $H_2SO_4$ solution than the commercial Pt/C catalyst, due to the coexistence of PtSn alloys and Sn oxides.

© 2009 Elsevier B.V. All rights reserved.

## 1. Introduction

Fuel cells are usually classified into low- and high-temperature fuel cells according to their operating temperature. Based on the fuel used in the low-temperature fuel cells, they can be classified as proton exchange membrane fuel cells (PEMFCs) using reformed hydrogen as fuel and direct methanol fuel cells (DMFCs) directly utilizing methanol as fuel. Low-temperature fuel cells, which operate in the 60–100 °C range and use a polymer membrane as the electrolyte, are an attractive energy source due to the low operating temperature and high energy density. These features have elevated low-temperature fuel cells as the most promising and attractive candidate for a wide variety of power applications ranging from portable and stationary power supplies to transportation. Regardless of their advantages such as low operating temperature and high energy density, there are still many obstacles to overcome before realizing commercial applications.

A Pt/C electrocatalyst so far is the best material to be used in low-temperature fuel cells. However, Pt, which is expensive and rare, is not the best catalyst for anode material owing to easy poisoning by the strongly adsorbed CO [1]. It is well known that methanol oxidation on a Pt/C catalyst occurs with the formation of adsorbed CO as intermediate, which becomes a poison on the active sites and significantly reduces the cell performance [1]. Thus, to produce a useful electrocatalyst, significant efforts have been made worldwide to decrease the amount of Pt used and to overcome the problem of CO poisoning [2–26]. The solutions that were introduced involve the use of secondary metals such as Ru [4–8], Sn [4,9–14], Mo [15,16], and Cr [4,17] to promote the catalytic activity and the oxidation of the chemisorbed CO [18]. Among the most active Pt-based alloy catalysts that have been considered for activity and CO tolerance, a PtRu alloy catalyst was studied in many research groups [4–8,19–21]. The addition of Ru to a Pt/C catalyst increases the CO tolerance of Pt metal in low-temperature fuel cell. Two models, which are the bifunctional model and the ligand model, have been proposed to explain the increased CO tolerance of Pt/C catalyst with the addition of Ru [19–21,17,23,24]. According to the bifunctional model [19–21,17], an oxygenated surface is created by dissociating water onto the Ru sites at lower potentials (0.2 V, NHE) than Pt, which promotes the oxidation of adsorbed CO to $CO_2$ and a decrease in the CO poisoning, thus improving the CO tolerance. Based on the ligand model [22,23], Ru changes the chemical properties of Pt at the surface such that the Pt–CO bond strength is reduced, and hence CO poisoning is minimized. Recently, utilization of PtSn/C catalyst as anode has been studied for methanol and ethanol oxidations in

* Corresponding author. Tel.: +82 2 880 7072; fax: +82 2 888 1604.
*E-mail address:* hilee@snu.ac.kr (H.-I. Lee).

0926-3373/$ – see front matter © 2009 Elsevier B.V. All rights reserved.
doi:10.1016/j.apcatb.2009.01.011

many groups [9–14,23–30]. In our previous work, the PtSn/C catalyst showed much higher activity for methanol and CO oxidations compared to the commercial Pt/C catalyst [14]. A PtSn/C catalyst was prepared to promote the oxidations of both methanol and CO chemisorbed on Pt sites containing Sn [9–14]. It was also reported that the onset potential of CO oxidation starts at a lower potential on PtSn/C catalyst than on PtRu/C and Pt/C catalysts [9,10,24–26]. Vigier et al. [31] reported that the presence of Sn activates the dissociative adsorption of ethanol, which leads to the breaking of the C–C bond, at lower potentials than Pt. Zhou et al. [24] showed that PtSn/C catalyst synthesized by a modified polyol method had higher activity for ethanol oxidation than a Pt/C catalyst. Jiang et al. [28] deduced that the unchanged lattice parameter of Pt in the $PtSnO_x$ catalyst is favorable to ethanol adsorption, and $SnO_x$ in the vicinity of Pt nanoparticles could conveniently offer oxygen species to remove the CO adsorbed on Pt sites. However, their synthesis processes were somewhat complicated and made commercial production less feasible.

In this study, we have devised a novel method for preparing PtSn/C catalyst and evaluated the resulting catalysts for methanol and CO oxidations as well as long-term durability. Specifically, we have focused on modifying the Pt/C catalyst by the addition of Sn, which results in the coexistence of PtSn alloys and $SnO_2$ close to Pt particles. It is expected that this catalyst system may increase activity and durability as anode for low-temperature fuel cell. The synthesis method employed in this study provided an easy and reproducible way for preparing of PtSn alloys and $PtSnO_2$ supported on carbon. The catalytic activity, physical and electrochemical properties of the PtSn/C catalysts were correlated and discussed.

## 2. Experimental

### 2.1. Catalyst preparation

20 wt% PtSn/C catalysts with the Pt/Sn atomic ratios of 5:1, 3:1, 1:1, and 1:3 were prepared by borohydride reduction and subsequent hydrothermal treatment. For the purpose of comparison, the loading amount of Pt metal in the commercial Pt/C(E-TEK) catalyst was fixed by 20 wt% in this study. To make a highly dispersed and highly stable solution, carbon black (Vulcan XC-72R, Carbot Co.) was treated with nitric acid at its boiling point (140 °C) [3,32,33]. This treatment of carbon with nitric acid introduces many organic functional groups, such as hydroxyl, carboxyl, and carbonyl on the surface of the carbon black [3,32,33]. Treatment of carbon black with boiling nitric acid is known to increase its hydrophilicity. Therefore, this treatment of carbon black makes it possible to easily disperse the carbon into a solution.

The precursors, chloroplatinic acid ($H_2PtCl_6{\cdot}6H_2O$, Acros Organics) and stannous chloride dihydrate ($SnCl_2{\cdot}2H_2O$, Junsei Chemicals), and pretreated carbon black were quantitatively dissolved and dispersed in the mixture of distilled water and methanol in a Teflon bottle, then 5 M NaOH solution was slowly added until the pH reached 11. With vigorous stirring, 0.01 g of sodium borohydride ($NaBH_4$, Junsei Chemicals) was dissolved in 30 ml of $H_2O$ and added drop-by-drop to the solution with a syringe pump (KD Scientific Inc.). The Teflon bottle was placed in a stainless steel vessel and sealed tightly. The hydrothermal treatment was performed in an oven at 150 °C for 3 h, and then the autoclave was cooled down to room temperature. After hydrothermal treatment, the solution was treated by adding 5 M HCl solution until the pH reached 2. The resulting suspension was filtered, washed with excess ethanol and distilled water, and then dried overnight in a vacuum oven at room temperature.

The samples were characterized by X-ray diffraction (XRD), thermogravimetry differential scanning calorimetry (TG-DSC), high-resolution transmission electron microscopy (HR-TEM), X-ray photoelectron spectroscopy (XPS), and evaluated with electrochemical techniques.

### 2.2. Physical characterizations

Structural characteristics of the synthesized powders were investigated by XRD (D8 ADVANCE, Bruker) using Cu Kα as the radiation source. For XRD, the working voltage and current were maintained at 40 kV and 30 mA, respectively. The $2\theta$ angular region between 20° and 80° was explored at a scan rate of 0.2 s $step^{-1}$. The average crystallite sizes and lattice parameters for the PtSn/C catalysts were evaluated according to the full width at half maximum (FWHM) and the angular position of the Gaussian-fitted Pt(2 2 0) peak, respectively. The width of the Pt(2 2 0) peak was used to calculate the average crystallite size according to Scherrer's equation [34]. And the Bragg formula [32] was employed to calculate the lattice parameters of the PtSn/C catalysts.

For the TG-DSC measurements, a thermal analyzer (SDT Q-600, TA Instruments) with an alumina sample pan was used; the measurements were conducted in the temperature range from 30 °C to 800 °C using an air flow of 100 ml $min^{-1}$.

The surface morphology of PtSn nanoparticles on carbon black was studied via HR-TEM (JEM-3010, JEOL) operated at 300 kV. The samples for TEM were prepared by adding a drop of the suspension, made by ultrasonically dispersing the catalyst in ethanol, onto a copper grid (200 mesh) covered with carbon film, and then evaporating the ethanol. The mean particle size, $d$, was calculated using the following equation:

$$d = \frac{\sum n_i d_i}{\sum n_i} \quad (1)$$

where $n_i$ is the frequency of the catalyst particles having diameter of size $d_i$.

The surface chemical state and bonding of the PtSn catalysts were analyzed by using XPS (Axis Utra, Kratos). The XPS analysis was conducted at 450 W, pass energy of 50 eV, and using Mg Kα radiation as the exciting source. The peak positions were corrected for sample charging by setting the C1s binding energy at 284.8 eV. The peak fitting of the XPS spectra was done using a Shirley function and Gaussian–Lorentzian functions. Peak areas of the XPS spectra were also estimated by calculating the integral of each peak after subtracting a Shirley background.

### 2.3. Electrochemical measurements

The electrochemical measurements were carried out in a half-cell using a potentiostat (PC4/750, Gamry Instruments). A conventional three-electrode cell, in which reference, counter, and working electrodes were separated, was used for the electrochemical measurements over the PtSn/C catalysts and a commercial Pt/C(E-TEK) catalyst. The catalyst ink was prepared by sonicating the catalyst with a 5% Nafion® solution (1100 EW, Du Pont) in isopropyl alcohol for approximately 30 min to form a slurry. The ratio of catalyst to Nafion® in the catalyst ink was 3:1. The substrate for the catalyst ink was a glassy carbon (GC) disk electrode (MF-2012, BAS) with a diameter of 6 mm, which was polished to a mirror finish with a 0.05 μm gamma alumina suspension (40-6301-016, Buehler) before each experiment. A drop of catalyst ink was dropped onto the surface of GC disk electrode and dried at room temperature. Each electrode was installed in a three-electrode cell with a platinum mesh electrode (219810, Princeton Applied Research) as the counter electrode and a KCl-saturated Ag/AgCl electrode (MF-2052, Bioanalytical System, Inc.) as the reference electrode, which was located as close as

possible to the working electrode. A three-electrode cell was filled with electrolyte solution and purged with nitrogen gas to remove oxygen dissolved in the electrolyte solution.

In this study, all of the potential readings were recorded with respect to a normal hydrogen electrode (vs. NHE). Before every electrochemical measurement, the potential was cycled between +0 and 1.2 V (vs. NHE) at 100 mV $s^{-1}$, to obtain a clean, active electrochemical surface. The $H_2$ adsorption/desorption curve was measured in the potential range between 0 and 1.2 V at 20 mV $s^{-1}$ in 0.5 M $H_2SO_4$ electrolyte solution purged with nitrogen at 25 °C. The methanol oxidation reaction (MOR) was performed at 20 mV $s^{-1}$ in a nitrogen-purged mixed solution of 2 M $CH_3OH$ and 0.5 M $H_2SO_4$ used as an electrolyte at 40 °C. CO stripping was carried out in a 0.5 M $H_2SO_4$ solution which was initially purged with nitrogen gas for 20 min, and then the adsorption of CO on the catalysts was performed by purging CO gas into the electrolyte solution at 0.1 V (vs. NHE) for 30 min. The residual CO in the solution was removed by subsequent nitrogen purging for 20 min. Finally, the CO stripping voltammetry was measured in the potential range of 0–1.2 V (vs. NHE) with a scan rate of 50 mV $s^{-1}$ at 25 °C.

### 2.4. Fuel cell tests

The membrane electrode assembly (MEA) for low-temperature fuel cell was fabricated from commercial Nafion® 112 membrane (DuPont) according to the standard membrane cleaning procedure [34–36]. The Nafion membrane was pretreated by successive dipping it in a 5 wt% $H_2O_2$ solution, distilled water, 8 wt% $H_2SO_4$ solution, and distilled water at 80 °C for 30 min each step. For preparation of the catalyst-coated membrane (CCM) [34], the catalyst ink was sprayed uniformly by a spray gun onto the pretreated membrane. The catalyst loadings of the anode and cathode were both 0.3 mg $cm^{-2}$ and the active surface area of a single-cell was 5 $cm^2$. A gas diffusion layer, based on carbon paper substrates (TGPH-060, Toray Inc.), was placed on the anode and cathode sides of the catalyst-coated membrane to form a single-cell. The MEA was mounted in a single-cell with stainless steel end plates and graphite carbon flow fields as current collectors.

Single-cell tests were carried out using the 3Pt1Sn/C and commercial Pt/C catalysts as the anode and the commercial Pt/C catalyst as the cathode. Pure $H_2$ and a mixture of $H_2$ and CO (10 ppm and 50 ppm) were used for anode gas and $O_2$ for cathode gas with a flow rate of 100 ml $min^{-1}$ at a cell temperature of 80 °C. These gases were humidified in a bubbling humidifier before entering the fuel cell. The humidification temperatures for anode and cathode gases were 90 °C and 85 °C, respectively. The IV characteristics of single-cells were performed using a commercial fuel cell test station (SMART II PEM/DM Hybrid Fuel Cell Test System, WonATech Co.).

## 3. Results and discussion

### 3.1. Physical characterizations

#### 3.1.1. TG-DSC analysis

The result of TG curves of the 20 wt% PtSn/C catalysts with the Pt/Sn atomic ratios of 3:1, 1:1, and 1:3 are shown in Fig. 1a, which indicates dramatic weight loss moves to higher temperature with increasing loading amounts of Sn. The shift of the weight loss to higher temperature is due to the lower amounts of Pt metal in the comparative sample, suggesting that the Pt nanoparticles on carbon catalyzed the oxidation of carbon. The second contribution is also enhanced with the addition of Sn. This should be due to the difference in capability of the carbon oxidation between Pt and Sn. Therefore, the second contribution could be enhanced with

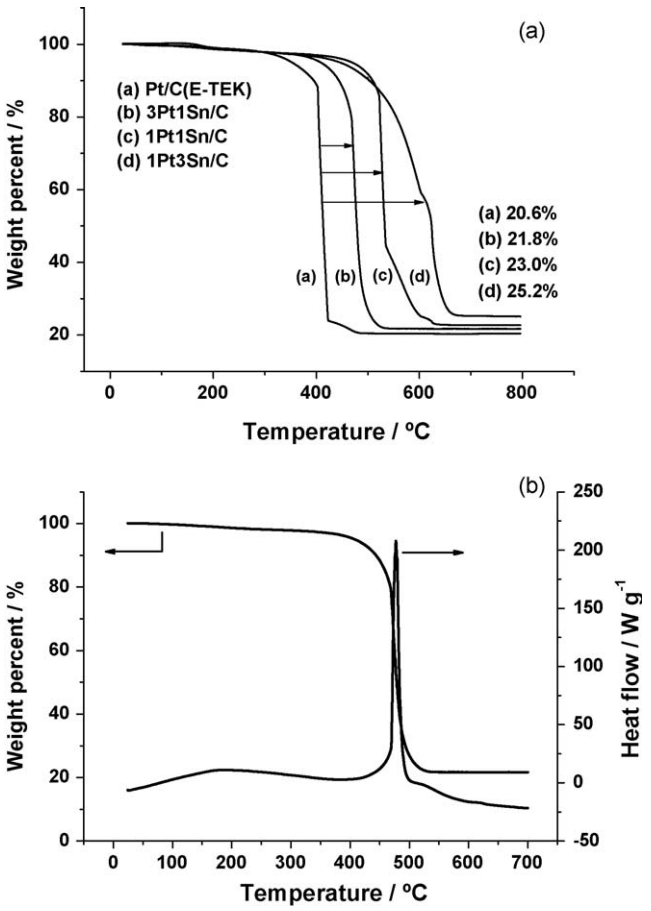


**Fig. 1.** (a) TG curves of the PtSn/C catalysts with the Pt/Sn atomic ratios of 3:1, 1:1, and 1:3, and the commercial Pt/C(E-TEK) catalyst and (b) TG-DSC curve of 3Pt1Sn/C catalyst.

increasing Sn content. The TG-DSC curve of the 3Pt1Sn/C sample is shown in Fig. 1b. The first endothermic peak at a temperature below 180 °C is ascribed to the removal of physisorbed water from the catalyst. The strong endothermic reaction with a dramatic weight loss at about 480 °C and 520 °C is attributed to the combustion of carbon to form $CO_2$. There were two weight loss peaks overlapped, which should be due to the different states of carbon. The combustion was completed at about 540 °C and left about 21.8% of the sample as residue due to the supported Pt and Sn. In comparison with the nominal loading, the TG determined metal loading is higher by about 1.8% due to the oxidation of Pt and Sn metals during the TG analysis. Based on the TGA results, the loading amounts of Pt and Sn were confirmed to be accurate. Thus, the preparation method employed guarantees the complete preparations of Pt and Sn as well as the full loading of Pt and Sn nanoparticles on a carbon support.

#### 3.1.2. XRD analysis

The XRD patterns of the 20 wt% PtSn/C catalysts synthesized by borohydride reduction and subsequent hydrothermal treatment are shown in Fig. 2. For comparison, the patterns of the commercial 20 wt% Pt/C(E-TEK) catalyst are also provided. The first broad peak at about 25° is associated with carbon as support material. As clearly indicated from the diffraction patterns of the PtSn/C catalyst in Fig. 2, both crystalline Pt and $SnO_2$ phases coexist. Also, there were no obvious peaks for Sn as shown in Fig. 2. The diffraction patterns of the PtSn/C catalysts exhibited the typical peaks for the face-centered cubic (fcc) structure of crystalline Pt. The peaks of $SnO_2$ phase at about 34° and 52° are also present in the

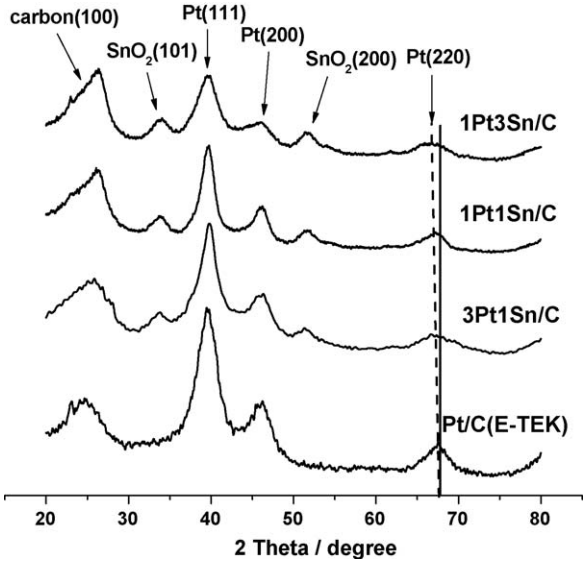


**Fig. 2.** X-ray diffraction patterns of the PtSn/C catalysts with the Pt/Sn atomic ratios of 3:1, 1:1, and 1:3, and the commercial Pt/C(E-TEK) catalyst.

diffraction patterns of the PtSn/C catalysts with the Pt/Sn atomic ratios of 3:1, 1:1, and 1:3. It can be also seen from Fig. 2 that the peaks of $SnO_2$ (1 0 1) and $SnO_2$ (2 1 1) phases become prominent as the Sn content increases. The width of Pt(2 2 0) peak is used to calculate the average crystallite size according to Scherrer's equation [34]:

$$L = \frac{0.9\lambda}{B_{1/2}\cos\theta} \quad (2)$$

where $L$ is the average crystallite size, $\lambda$ is the X-ray wavelength (1.54 Å for Cu Kα radiation), $B_{1/2}$ is the full width at half maximum, and $\theta$ is the angle corresponding to the peak maximum.

In addition, we calculated the lattice parameter ($a_{fcc}$) values for the PtSn/C catalysts by using the Pt(2 2 0) peaks [32]:

$$a_{fcc} = \frac{\sqrt{2}\lambda_{K\alpha 1}}{\sin\theta} \quad (3)$$

The average crystallite size and lattice parameter obtained from XRD patterns are summarized in Table 1. The average crystallite sizes and lattice parameters for the PtSn/C catalysts were evaluated according to the FWHM and the angular position of the Gaussian-fitted Pt(2 2 0) peaks, respectively. It shows that the average crystallite sizes of the PtSn/C catalysts were smaller than that of the commercial Pt/C catalyst. It can be seen from Table 1 that the addition of Sn to Pt/C catalyst increases the lattice parameter of Pt/C catalyst as a result of the Pt(2 2 0) peak shifting to lower positions. This increase in the lattice parameter in the presence of PtSn alloys may be the reason that allows easy adsorption and dissociation of methanol, thus increasing the activity for methanol oxidation at lower potentials. In addition, the presence of $SnO_2$ is also suspected to play a very important role in methanol and CO oxidations at lower potentials [37]. We have focused on modifying the Pt/C catalyst by the addition of Sn, which results in the existence of not only PtSn alloy but also $SnO_2$ close to Pt particles. PtSn nanoparticles deposited on a carbon support were prepared by borohydride reduction. In order to induce the coexistence of highly crystalline PtSn alloy as well as $PtSnO_2$, hydrothermal process which involves high temperature and high pressure was required. The physical contact between $SnO_2$ and Pt particles would be an essential requirement for a synergistic effect of $SnO_2$ on the Pt, as Crabb et al. have proposed [25].

The Pt(2 2 0) peak of the PtSn/C catalysts shifts slightly to lower $2\theta$ position with increasing Sn content compared to that of the commercial Pt/C catalyst. This result suggests the incorporation of Sn in the fcc structure of Pt causes the formation of the PtSn alloys. Since the radius of the Sn atom ($R_{Sn}$ = 0.161 nm) is larger than that of the Pt atom ($R_{Pt}$ = 0.139 nm), the substitution of Pt with Sn would lead to an expansion of the unit cell volume. It is worthwhile to note that the lattice parameter of the PtSn/C catalysts on XRD patterns appears to increase linearly with Sn content. Later, we will discuss about this tendency in relation to the catalytic activity of PtSn/C catalysts.

Especially, from the lattice parameters of the PtSn/C catalysts summarized in Table 1, we can note that the lattice parameter of the 3Pt1Sn/C catalyst ($a_0$ = 0.3953 nm) is smaller than that of the bulk Pt3Sn1 solid solution ($a_0$ = 0.4000 nm) previously reported in elsewhere [26,34]. This would originate from the several reasons such as the partial alloying of Sn, the metal-support interaction, and size effect [33]. However, it is due mainly to the partial substitution of Pt with Sn in the home-made 3Pt1Sn/C catalyst (partially alloyed), than that in bulk PtSn solid solution (fully alloyed). According to Kuznetsov et al. [38], PtSn alloys follow Vegard's law while taking the values of the lattice parameters of the bulk Pt3Sn1 and pure Pt. It was estimated that the atomic fraction of Sn alloyed in the PtSn/C catalyst is about 0.11. The alloyed Sn content in the PtSn/C catalyst is much lower than its nominal values, due to the partial alloying of Sn. Then, a considerable amount of non-alloyed Sn should be in the PtSn/C catalyst, very likely in the oxide form. In the case of our home-made PtSn/C catalyst, the presence of Sn oxide was observed in the XRD patterns (Fig. 2). Especially, we confirmed that Sn is mostly about 45% in an oxidized state from XPS spectrum (see Table 2). Therefore, we can insist that most of non-alloyed Sn might exist as 'oxide form' in the home-made PtSn/C catalysts.

### 3.1.3. HR-TEM analysis

A HR-TEM image of the 3Pt1Sn/C catalyst is shown in Fig. 3, which illustrated that the nanoparticles are uniformly dispersed on the surface of every carbon support grain. The average particle size for the PtSn/C catalysts with different Pt/Sn atomic ratios is given in Table 1, which is consistent with XRD data. Most of the PtSn

**Table 1**
Physical properties of the PtSn/C and commercial Pt/C(E-TEK) catalysts calculated from the XRD and HR-TEM data.

| Sample | Lattice parameter[a] (nm) | Mean particle size (nm) | |
|---|---|---|---|
| | | XRD[b] | TEM[c] |
| Pt/C(E-TEK) | 0.3931 | 2.8 | 3.0 |
| 3Pt1Sn/C | 0.3953 | 2.2 | 2.3 |
| 1Pt1Sn/C | 0.3983 | 2.4 | 2.4 |
| 1Pt3Sn/C | 0.4018 | 1.8 | 2.1 |

[a] The lattice parameter was calculated from Gaussian-fitted Pt(2 2 0) peak $2\theta$ position according to Fragg formula.
[b] The mean particle size was calculated from Gaussian-fitted Pt(2 2 0) peak according to Scherrer formula.
[c] The mean particle size was calculated by measuring the sizes of 150 randomly chosen particles form TEM images.

**Table 2**
Pt 4f and Sn 3d XPS spectra of the 3Pt1Sn/C catalyst.

| Species | Binding energy of Pt ($4f_{7/2}$) | Relative intensity (%) | Species | Binding energy of Sn ($4d_{3/2}$) | Relative intensity (%) |
|---|---|---|---|---|---|
| Pt(0) | 71.98 | 67.9 | Sn(0) | 485.98 | 54.7 |
| Pt(II) | 73.43 | 24.1 | Sn(II/IV) | 486.70 | 45.3 |
| Pt(IV) | 74.72 | 8 | | | |

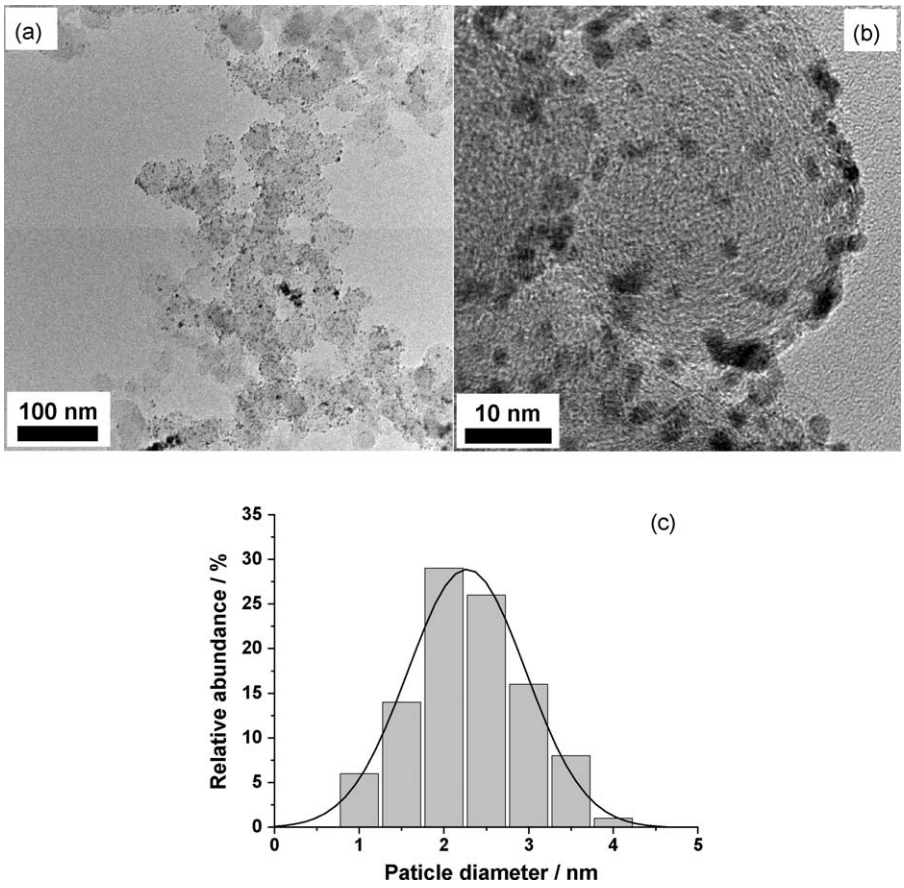


**Fig. 3.** (a) TEM and (b) HR-TEM images and (c) the diagram of particle size distribution of the 3Pt1Sn/C catalyst.

nanoparticles are spherical in shape without aggregation and have a narrow particle size distribution. The particle size distributions of the PtSn nanoparticles were obtained by measuring the sizes of 150 randomly chosen particles from a HR-TEM image. From Fig. 3a, the 3Pt1Sn nanoparticles are well-dispersed on carbon support with a narrow particle size distribution (Fig. 3c). Base on the HR-TEM images of the 3Pt1Sn/C catalyst, as in the one shown in Fig. 3b, the 3Pt1Sn nanoparticles dispersed on the surface of each carbon support grain are very uniform in size; their average particle size was around 2.3 nm agreeing well with the data of XRD.

*3.1.4. XPS analysis*

Fig. 4a shows the XPS spectrum of Pt 4f, which can be deconvoluted into three components, ascribed to Pt(0), Pt(II), and Pt(IV). The most intense peak at around 71.9 eV is assigned to metallic Pt(0). The slight shift in the bulk metallic Pt(0) to higher binding energies is attributed to a significant contribution from metal-support interaction and nano-size effect [39,40]. The second peak is assigned to Pt(II) as in PtO and $Pt(OH)_2$, and the third one to Pt(IV) [41]. The XPS spectrum of Sn 3d is shown in Fig. 4b, which was deconvoluted into two components. The first peak at lower binding energy can be attributed to the presence of Sn(0) and the other one corresponds to oxidized species of Sn(II/IV). Discriminating between Sn(II) and Sn(IV) with XPS is difficult. The binding energies of Sn are slightly higher than reference data, due to interactions between Sn and Pt, higher Sn content, and nano-size effect. From these data, it is confirmed that Sn is mostly in an oxidized state. Note that the presence of Sn oxide species was also observed in the XRD patterns at 34° and 52° (Fig. 2). The binding energies and the relative concentrations of Pt and Sn species in the 3Pt1Sn/C catalyst are reported in Table 2. When $SnO_2$ nanoparticles are located in the vicinity of Pt nanoparticles, it is expected that $SnO_2$ will promote methanol and CO oxidations on the Pt sites, improving the catalytic activity. Therefore, the 3Pt1Sn/C catalysts synthesized by borohydride reduction with subsequent hydrothermal treatment, which are deposited on a carbon support, can be expected to show better catalytic activity and CO tolerance in low-temperature fuel cell.

*3.2. Electrochemical characterizations*

*3.2.1. $H_2$ adsorption/desorption for electrochemical surface active area*

In order to obtain the voltammograms of $H_2$ adsorption/desorption, the potential was cycled between 0 and 1.2 V (vs. NHE) at 20 mV $s^{-1}$ in a nitrogen-purged 0.5 M $H_2SO_4$ electrolyte solution at 25 °C. The curves stabilized after 10 cycles. Fig. 5 shows the $H_2$ adsorption/desorption curves of the PtSn/C and commercial Pt/C catalysts. The catalysts exhibited well-defined $H_2$ adsorption/desorption peaks in the potential region of ~0 to 0.3 V (vs. NHE) and the $O_2$ adsorption/desorption peaks species at around 0.7 and 1.0 V (vs. NHE), which are in a good agreement with values reported in the literature [42,43]. The PtSn/C catalysts do not show a distinct $H_2$ adsorption/desorption region in comparison with the commercial Pt/C catalyst due to alloying between Pt and Sn [40,44,45]. Moreover, the cyclic voltammogram curves of the PtSn/C catalysts show an increase in current density at double layer as the Sn content increases, which could be related to Sn oxide species [40,44,45]. The high capacitive charging current in double layer region has been usually ascribed to the activation of $H_2O$ on Sn and $SnO_2$ species on the PtSn/C catalysts [44]. The small peaks that appear around 0.5 and 0.7 V may be attributed to the $O_2$ adsorption/desorption from the dissociation of water onto Sn oxide [9,10,14,22], which may be attributed to the presence of Sn

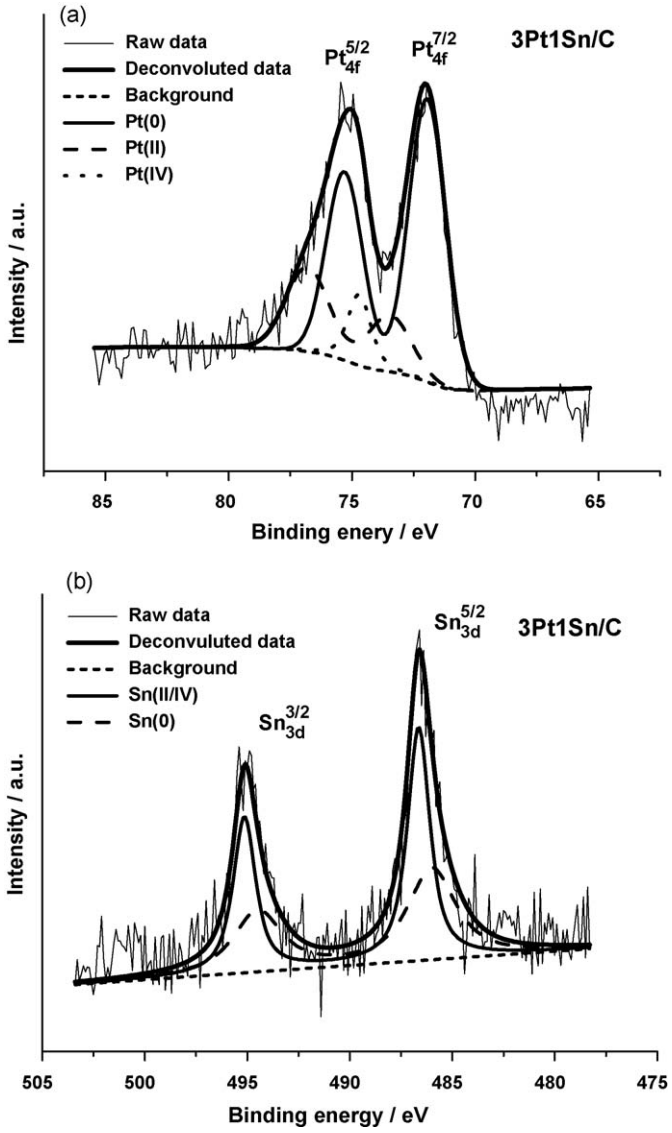


**Fig. 4.** (a) Pt 4f and (b) Sn 3d XPS spectra of the 3Pt1Sn/C catalyst.

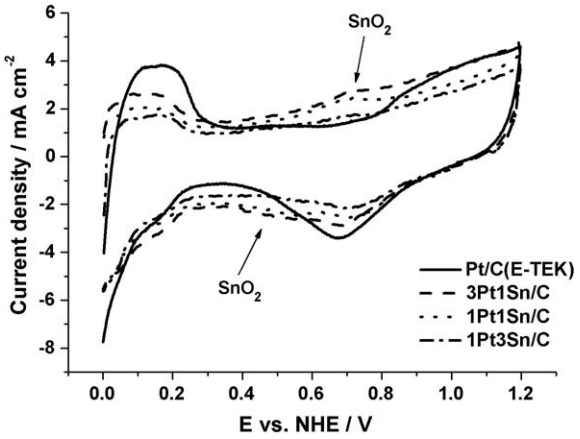


**Fig. 5.** Cyclic voltammograms of $H_2$ adsorption–desorption on the PtSn/C catalysts with Pt/Sn atomic ratio of 3:1, 1:1 and 1:3, and commercial Pt/C(E-TEK) catalyst in 0.5 M $H_2SO_4$ solution at a scan rate of 20 mV $s^{-1}$ at 25 °C.

oxide species (observed in the XRD patterns, Fig. 2). As already mentioned, the Sn oxide species are very important to methanol and CO oxidations at lower potentials [37]. The curves have also been used to estimate the electrochemical active surface area (EAS) of the PtSn/C and commercial Pt/C catalysts from the integrated charge in the $H_2$ desorption region [6,42]. The EAS value can be calculated from the following equation:

$$\mathrm{EAS}\,(\mathrm{m^2\,g^{-1}}) = \frac{Q_H}{0.21 \times [\mathrm{Pt}]} \quad (4)$$

where $Q_H$ (mC $cm^{-2}$) represents the charges exchanged during the desorption of hydrogen on the Pt surface, [Pt] (mg $cm^{-2}$) is the Pt loading in the electrode and 0.21 is the charge required to oxidize a monolayer of hydrogen on the Pt surface [46].

The estimated EAS values of the PtSn/C catalysts were summarized in Table 3. The calculated EAS value of the 3Pt1Sn/C catalyst was higher than those of the 1Pt1Sn/C and 1Pt3Sn/C catalysts. The high EAS value is likely due to the presence of nano-sized and well-dispersed PtSn particles on the carbon support, which was evidenced in the TEM images (Fig. 3).

### 3.2.2. Activity of the PtSn/C catalysts for methanol oxidation reaction

In order to evaluate the PtSn/C catalysts for methanol oxidation, a nitrogen-purged mixed solution of 2 M $CH_3OH$ and 0.5 M $H_2SO_4$ was used as the electrolyte solution at 40 °C. The values of current were normalized by both the loading amount and the surface area of the Pt metal, considering that methanol adsorption and dehydrogenation occurs only on the Pt sites at room temperature [47–49]. In order to evaluate the economic efficiency, the current densities are generally normalized by the amount of loaded metal ($(\mathrm{mA\,mg_{Pt}^{-1}})$) to compare the activity of different catalysts. Though the mass-normalized current density represents the economic efficiency of the catalyst, it does not take into account the surface area of the active metal sites. The area-normalized current densities were obtained by dividing the measured currents by calculated electrochemical surface. The area-normalized current density represents the intrinsic activity of the active sites in the electrocatalysts.

The mass- and area-normalized current densities of methanol oxidation on the PtSn/C and commercial Pt/C catalysts are shown in Fig. 6. The 3Pt1Sn/C catalyst shows the highest activity for methanol oxidation, owing to the slight increase in Pt lattice parameter favorable to methanol adsorption and the presence of Sn oxide in the vicinity of Pt particles. Especially, the area-normalized current density at 0.6 V for the 3Pt1Sn/C catalyst is about 3-fold that of the commercial Pt/C catalyst. The PtSn/C catalysts show the same trend in order between mass- and area-normalized current densities. The difference in gaps of the two defined current densities is due to the different metal dispersion on the carbon supports and the electronically and structurally effective change of metal surface. Therefore, the current densities of methanol oxidation on the PtSn/C catalysts sharply increase in the region around 0.4 V (vs. NHE), where as for the commercial Pt/C

**Table 3**
Electrokinetic parameters on the PtSn/C and commercial Pt/C(E-TEK) catalysts.

| Sample | $EAS_{H_2}$ [a] ($m^2\,g^{-1}$) | Mass activity @ 0.6 V [b] ($\mathrm{mA\,mg_{Pt}^{-1}}$) | Area activity @ 0.6 V [b] ($\mu\mathrm{A\,cm_{Pt}^{-2}}$) | Max peak position [b] (V) |
|---|---|---|---|---|
| Pt/C(E-TEK) | 42.3 | 24.7 | 58.3 | 0.84 |
| 3Pt1Sn/C | 28.5 | 56.7 | 201.8 | 0.86 |
| 1Pt1Sn/C | 24.3 | 37.1 | 154.5 | 0.86 |
| 1Pt3Sn/C | 17.7 | 14.2 | 80.1 | 0.84 |

[a] The EAS data were taken from the CVs shown in Fig. 5.
[b] The activity data were taken from the CVs shown in Fig. 6.

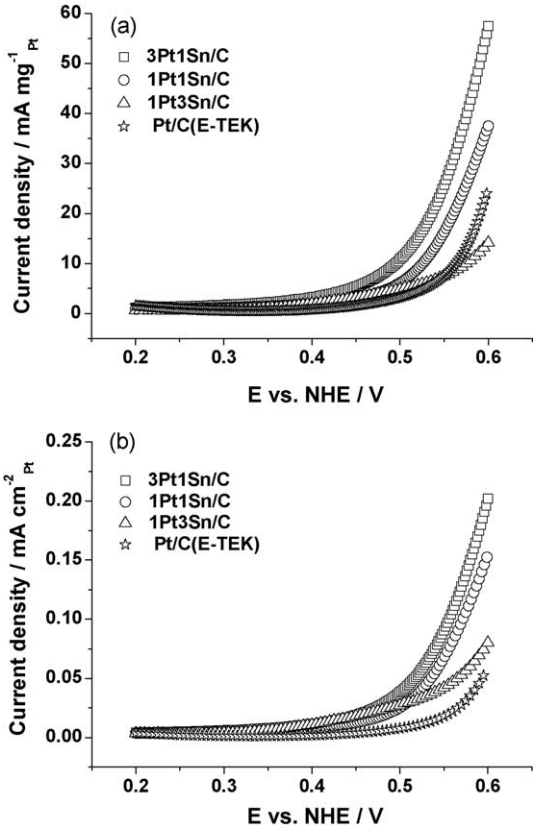


**Fig. 6.** (a) Mass- and (b) area-normalized cyclic voltammograms of methanol oxidation on the PtSn/C catalysts with the Pt/Sn atomic ratios of 3:1, 1:1, and 1:3, and the commercial Pt/C(E-TEK) catalyst in 2 M $CH_3OH$ + 0.5 M $H_2SO_4$ solution at a scan rate of 20 mV $s^{-1}$ at 25 °C.

catalyst the current increases slightly at around 0.55 V (vs. NHE). The onset potential of methanol oxidation is lower for the PtSn/C catalysts than for the commercial Pt/C catalyst [9,10,14,22]. This indicates that the energy required for methanol oxidation on the PtSn/C catalysts is lower, which may be attributed to both the electronic interaction between Pt and Sn (electronic effect) and the changes in the Pt lattice parameter (structure effect) due to the addition of Sn [37,50]. The presence of alloyed Sn, which expands the lattice, allows methanol to be adsorbed and dissociated at lower potentials than that observed on the commercial Pt/C catalyst [24]. Also, the presence of Sn oxide in the vicinity of Pt particles may be attributed to promote the methanol oxidation at lower potentials. Therefore, Sn or Sn oxide improves the methanol oxidation at lower potentials and increases the reaction rate. In this study, the 3Pt1Sn/C catalyst is suggested to be a more suitable catalyst for methanol oxidation in comparison with the 1Pt1Sn/C, 1Pt3Sn/C, and commercial Pt/C catalysts. Table 3 summarizes the electrochemical properties of the 3Pt1Sn/C and commercial Pt/C catalysts.

We considered that the changes of catalytic activity and lattice parameter with Sn content into the PtSn/C catalysts. As shown in Fig. 7, with increasing the Sn content, the lattice parameter linearly increases, whereas the catalytic activity shows a volcano curve. For the dependency of the catalytic activity, we divided the catalytic activity dependence into two regions of A and B as shown in Fig. 7. In the case of 'region A', the catalytic activity of PtSn/C catalyst for methanol oxidation dramatically increases by the addition of Sn content up to 25 at.% into Pt/C catalyst. Especially, 3Pt1Sn/C catalyst that has a lattice parameter around 0.3953 nm shows the best catalytic activity due to the proper expansion of lattice parameter and the appropriate existence of Sn oxide. The proper expansion of lattice parameter in the PtSn alloy may be main

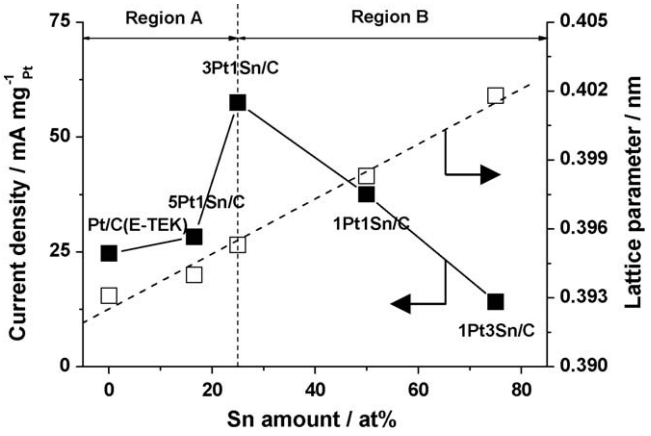


**Fig. 7.** Changes of catalytic activity and lattice parameter with different atomic percentage of Sn in the PtSn/C catalysts.

reason that allows easy adsorption and dissociation of methanol, thus improving cell performance. In addition, the appropriate existence of Sn oxide in the vicinity of Pt particles, may act as a promoter for methanol oxidation rather than as active site itself. On the other hand, in the 'region B' of higher Sn content up to 75 at.%, the catalytic activity for methanol oxidation decreases despite of the increase of lattice parameter by adding Sn. In particular, the catalytic activity of 1Pt3Sn/C catalyst shows the lowest among the catalysts in this study. This would be due to small amount of Pt as main active site and excessive amount of Sn oxide which does not more act as a promoter at this Sn content. From the experimental findings, we can conclude that the catalytic activity of PtSn/C catalyst might be determined by two effects of lattice parameter and Sn oxide due to the addition of Sn into the Pt/C catalyst. In other words, there is a critical value of Sn content, up to which the catalytic activity increases due to the expanded lattice parameter and the Sn oxide formed at the adjacent to Pt, but above which the activity falls due to the lack of main active site and the excessive Sn formation. Consequently, in the present study, the optimum value of Sn content was 25 at.% resulted from 3Pt1Sn/C which gives the best catalytic activity as shown in Fig. 7.

### 3.2.3. CO stripping test

The activities of the PtSn/C and commercial Pt/C catalysts for CO oxidation were investigated by CO stripping voltammetry in 0.5 M $H_2SO_4$ at 50 mV $s^{-1}$, and the results are shown in Fig. 8. For CO stripping voltammetry, CO was adsorbed on the catalysts at 0.1 V

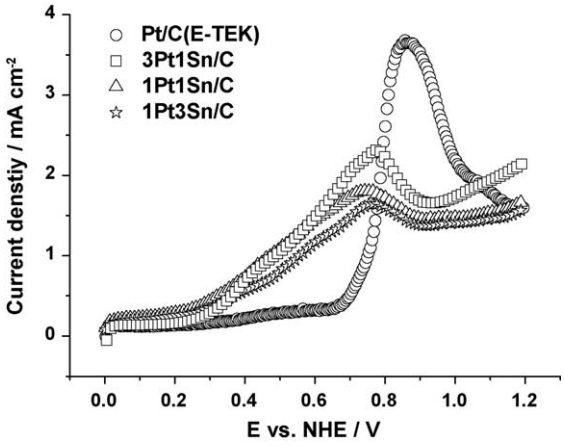


**Fig. 8.** CO stripping voltammograms of the PtSn/C catalysts with the Pt/Sn atomic ratios of 3:1, 1:1, and 1:3, and the commercial Pt/C(E-TEK) catalyst, obtained in 0.5 M $H_2SO_4$ at a scan rate of 50 mV $s^{-1}$ at 25 °C.

(vs. NHE) for 30 min. Fig. 8 shows the first scan of the PtSn/C and commercial Pt/C catalysts with an adsorbed CO. The onset potential for CO oxidation occurs at around 0.64 V (vs. NHE), and the maximum of CO oxidation peaks at around 0.86 V (vs. NHE) for the commercial Pt/C catalyst. On the other hand, the onset potential for CO oxidation starts at around 0.23 V (vs. NHE) and the maximum peaks at around 0.75 V (vs. NHE) for the PtSn/C catalysts. The onset potential and maximum peak of CO oxidations are lower for the PtSn/C catalysts compared to the commercial Pt/C catalyst. The shift of onset potential to lower values in CO stripping voltammetry for the PtSn/C catalysts is in agreement with previous works [8,10,22–25]. This indicates that the activity of the PtSn/C catalysts for CO oxidation is superior to that of the commercial Pt/C catalyst. It appears that Sn has the ability to promote the oxidation of adsorbed CO at lower potentials [25–27,51,52]. In other words, the Sn sites are always free to adsorb $OH^-$ species, which prefer to be adsorbed mostly onto Sn sites rather than on Pt sites. Moreover, Sn or Sn oxide are able to form oxygen-containing species at lower overpotentials than Pt. Therefore, the shift of onset potential on the PtSn/C catalysts may be attributed to the presence of oxygenated species onto Sn or Sn oxide sites at lower potentials, compared to the commercial Pt/C catalyst [8,25–27,52]. The predominant activities of the PtSn/C catalysts can be explained by a bifunctional mechanism: $OH^-$ species formed by dissociative adsorption of water and adsorbed onto Sn or Sn oxide sites could oxidize the CO adsorbed onto Pt to $CO_2$ at lower potentials [9,10,14]. When Sn or Sn oxides are located in the vicinity of Pt, Sn or Sn oxides could offer oxygen species to remove the CO adsorbed onto Pt sites, resulting in the promotion of the CO oxidation. Moreover, the range of CO oxidation of the PtSn/C catalysts is wider than that of the commercial Pt/C catalyst. The onset potential of CO oxidation is all the same for the PtSn/C catalysts in spite of different amounts of Sn content. Crabb et al. [25] insisted that the onset potential of CO oxidation is lowered with addition of a small amount of Sn but shows little effect in terms of potential shift as further quantities of Sn are added. According to Massong et al. [53], this result is due to the presence of adsorbed linearly bonded CO and bridge-bonded CO on Pt sites. They claimed that bridge-bonded CO could be oxidized at lower potentials on the PtSn/C catalysts compared to the commercial Pt/C catalyst. This suggests that the role of Sn is mainly to promote the cleavage of C–H bond and to improve the removal of $CO_{ad}$ species onto the active Pt sites during the methanol oxidation, which consequently enhances the methanol oxidation.

### 3.2.4. Single-cell performances

In order to understand the enhanced cell performance and CO tolerance of the 3Pt1Sn/C catalysts showing the best activity for methanol and CO oxidations in the half-cell test, single-cell tests were carried out for low-temperature fuel cell using the 3Pt1Sn/C and commercial Pt/C catalysts as anodes and the commercial Pt/C catalyst as cathode. Hydrogen gas and a mixture of $H_2$ and CO (10 ppm and 50 ppm) were used for the anode gas and $O_2$ for the cathode gas at a cell temperature of 80 °C. Fig. 9 shows *I–V* curves for the 3Pt1Sn/C and commercial Pt/C catalysts. The open circuit voltages (OCVs) of the single-cells using both the 3Pt1Sn/C and commercial Pt/C catalysts are almost similar. However, the 3Pt1Sn/C catalyst shows a lower polarization loss than the commercial Pt/C catalyst. As indicated from the methanol and CO oxidations in the half-cell test, the 3Pt1Sn/C catalyst has a better performance than the commercial Pt/C catalyst in the pure $H_2$ and $H_2$ and CO mixture gas. Especially, in the case of 50 ppm CO-containing $H_2$ gas, although the performances for both catalysts drop considerably, the differences in their performances is much larger compared to that of the pure $H_2$ and 10 ppm CO-containing $H_2$ gas. That is, the performance with $H_2$ + 50 ppm CO for the 3Pt1Sn/C catalyst is much better than for the pure Pt catalyst. Hence, we suggest that Sn has the ability to enhance the oxidation of adsorbed CO due to the electronic interaction between Pt and Sn (electronic effect) and the changes in the Pt lattice parameter (structure effect) due to the addition of Sn.

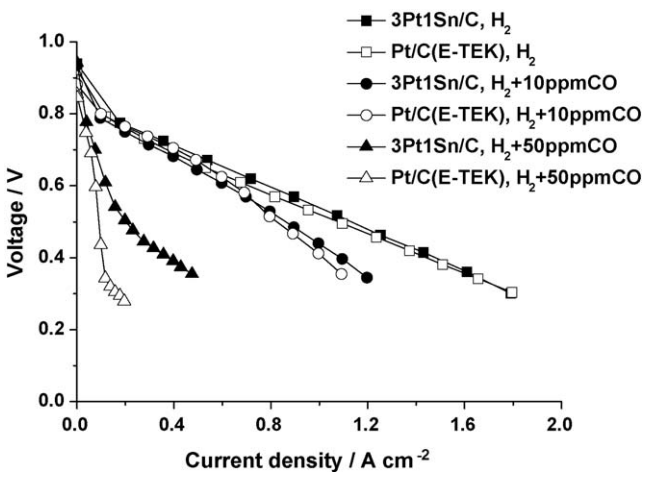


**Fig. 9.** Polarization curves for the 3Pt1Sn/C and commercial Pt/C(E-TEK) catalysts for anodes and the commercial Pt/C(E-TEK) catalyst for cathode under operating conditions comprising of $H_2$ and a mixture of $H_2$ and CO (10 ppm and 50 ppm) as anode gases and $O_2$ as cathode gas at 80 °C and 1 atm.

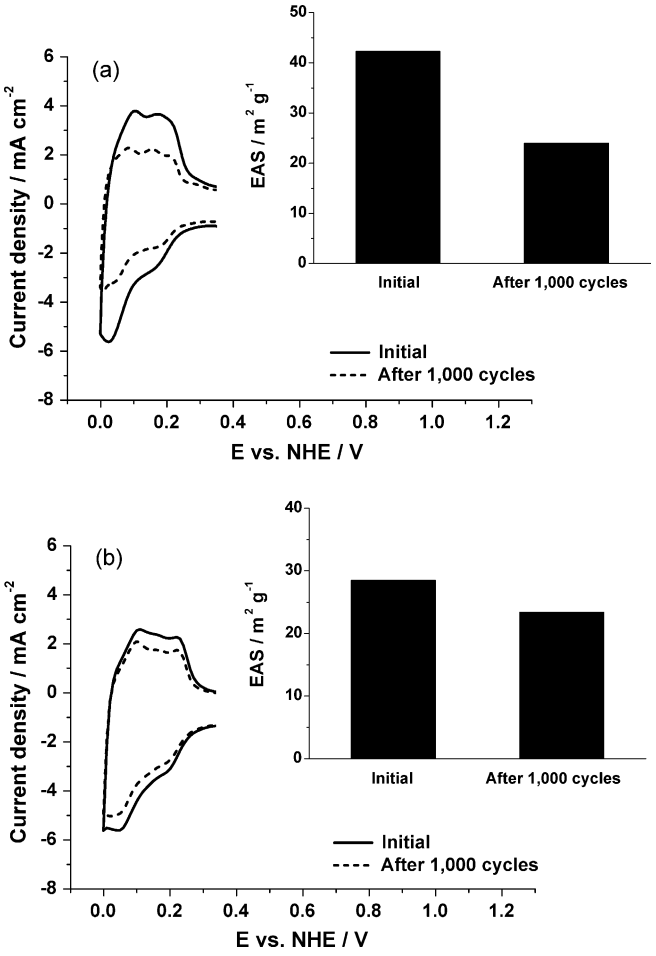


**Fig. 10.** Cyclic voltammograms of $H_2$ adsorption–desorption on the 3Pt1Sn/C and commercial Pt/C(E-TEK) catalysts before and after 1000 potential cycles.

*3.2.5. Accelerated stability test*

Accelerated stability tests of the 3Pt1Sn/C and the commercial Pt/C catalysts were carried out by a consecutive sweep from 0 to 1.2 V at 50 mV $s^{-1}$ for 1000 potential cycles in a 0.5 M $H_2SO_4$ solution. The voltammograms of $H_2$ adsorption/desorption was used to determine the change of the Pt active surface area for the 3Pt1Sn/C and commercial Pt/C catalysts by measuring $H_2$ desorption regions before and after 1000 potential cycles (Fig. 10). It can be seen from Fig. 10a that the $H_2$ desorption region for the commercial Pt/C catalyst decreases rapidly (about 43%) after the accelerated stability test, indicating a remarkable decrease of the Pt active surface area due to Pt sintering, the dissolution of Pt metal, and the oxidation of the carbon support [54,55]. On the other hand, the $H_2$ desorption region for the 3Pt1Sn/C catalyst after the accelerated stability test shows no significant variation, indicating no considerable decrease of the Pt active surface area (Fig. 10b). This finding shows that the 3Pt1Sn/C catalyst has a better durability in the acidic solution compared to the commercial Pt/C catalyst due to the coexistence of PtSn alloys and Sn oxide. Furthermore, from the TEM images before and after the accelerated stability test (Fig. 11), the particle size of the commercial Pt/C catalyst was increased from 2.8 nm to 5.3 nm after 1000 potential cycling (Fig. 11a and b). Thus, the main reason for the decrease in the Pt active surface area is confirmed to be the sintering of the Pt particles as evident from the TEM images. Zaragoza-Martin et al. [54] insisted that the decrease in the Pt surface area results form the aggregation of Pt particles which can be produced by the effect of the applied potential and the oxidation of the carbon support. On the other hand, the TEM image of the 3Pt1Sn/C catalyst shows an increase of particle size from 2.3 nm to 3.1 nm after 1000 potential cycling (Fig. 11c and d). The increase in the particle size of the 3Pt1Sn/C catalyst is very small compared to that of the commercial Pt/C catalyst. Therefore, the coexistence of PtSn alloys and Sn oxide seemed to play a very important role in the enhancement of the sintering resistance.

The enhanced electrocatalytic activity and durability of the PtSn/C catalysts for methanol and CO oxidations can be explained by the bifunctional effect and ligand effect of the electrocatalyst. Methanol prefers to bind with Pt atoms, and dehydrogenates to form $CO_{ad}$ intermediates as the main poisoning species onto the Pt atoms (5). Due to the higher affinity of Sn or Sn oxides toward oxygen-containing species, an oxygenated surface as the $OH_{ad}$ species is created by dissociating water on the Sn or Sn oxides sites at lower potentials than on Pt sites ((6a) and (6b)), which promotes

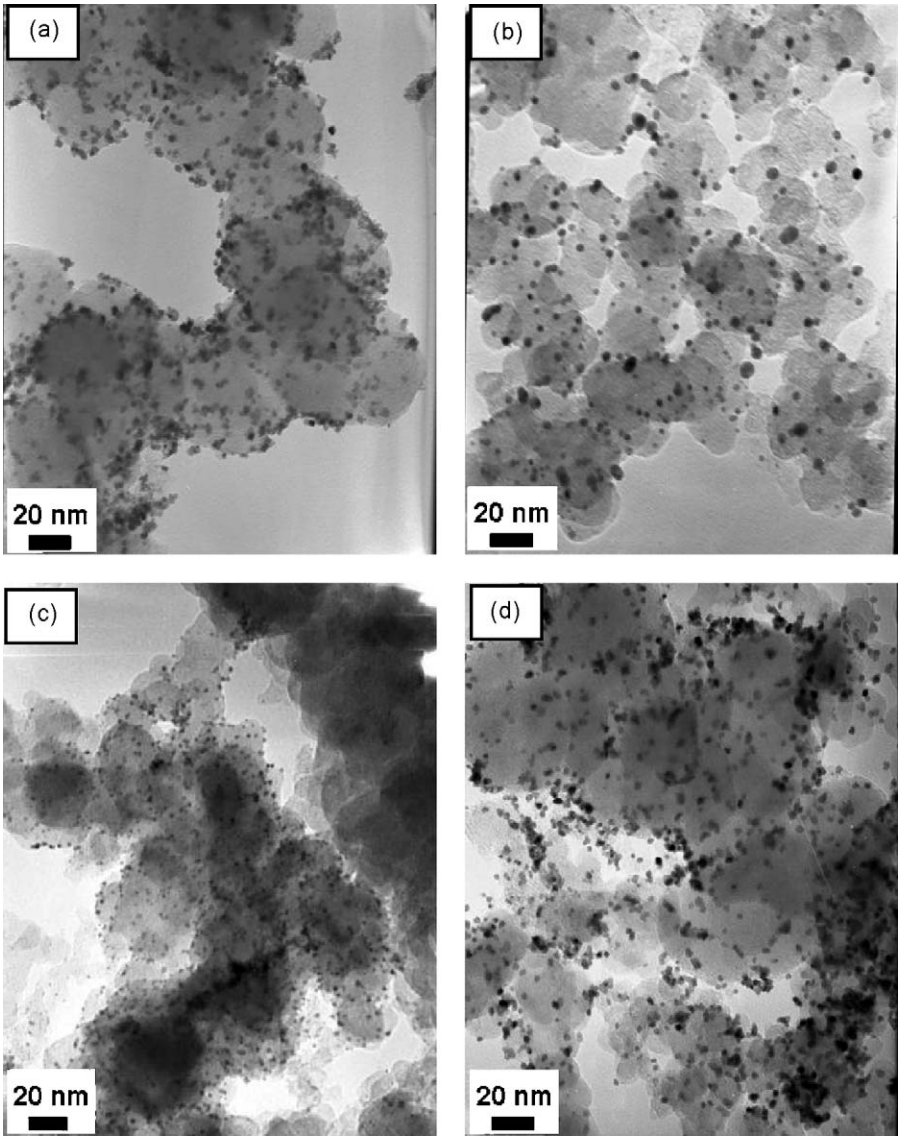


**Fig. 11.** TEM images of the (a and b) commercial Pt/C(E-TEK) and (c and d) 3Pt1Sn/C catalysts (a and c) before and (b and d) after 1000 potential cycles.

the oxidation of adsorbed CO to $CO_2$ and results in a decrease in the CO poisoning ((7a) and (7b)), thus improving the CO tolerance. Moreover, Sn changes the chemical properties of Pt at the surface such that the Pt–CO bond strength is reduced, and hence CO poisoning is minimized. Both of these effects lead to the higher catalytic activity and durability for the overall methanol oxidation process on the PtSn/C catalyst compared to the Pt/C catalyst:

$$Pt + CH_3OH_{ad} \rightarrow Pt{-}CO_{ad} + 4H^+ + 4e^- \quad (5)$$

$$Sn + H_2O \rightarrow Sn{-}OH_{ad} + H^+ + e^- \quad (6a)$$

$$SnO_2 + H_2O \rightarrow SnO_2{-}OH_{ad} + H^+ + e^- \quad (6b)$$

$$Pt{-}CO_{ad} + Sn{-}OH_{ad} \rightarrow CO_2 + H^+ + e^- \quad (7a)$$

$$Pt{-}CO_{ad} + SnO_2{-}OH_{ad} \rightarrow CO_2 + H^+ + e^- \quad (7b)$$

The new synthesis used in this study provided an easy and reproducible procedure for the preparation of coexistent PtSn alloys with Sn oxide, supported on carbon support. The predominant activity and durability of the PtSn nanoparticles suggest that the PtSn/C catalyst may be a good alternative as anode in low-temperature fuel cell.

## 4. Conclusions

In the present study, PtSn/C electrocatalyst was easily prepared by a continuous two-step process and was subsequently used as anode material in low-temperature fuel cell. From both XRD and HR-TEM results, it was found that the PtSn nanoparticles, with average particle size of 2.3 nm, were uniformly well-dispersed on the carbon support. The 3Pt1Sn/C catalyst showed the highest level of catalytic activity for methanol oxidation among the prepared samples and commercial Pt/C catalyst. In the $CH_3OH$ and CO oxidations, the onset potential with the 3Pt1Sn/C catalyst started at lower potentials, which may be attributed to both the electronic interaction between Pt and Sn (electronic effect) and the changes in the Pt lattice parameter (structure effect) due to the addition of Sn. Therefore, the addition of Sn was supposed to prevent CO from the poisoning of the active Pt sites through easier oxidation of adsorbed CO. As demonstrated, in the $CH_3OH$ and CO oxidations, the 3Pt1Sn/C catalyst showed a higher performance and power densities compared to the commercial Pt/C catalyst under $H_2$, as well as under a mixture of $H_2$ and CO in the performed single-cell tests. Furthermore, the coexistence of PtSn alloys and $PtSnO_2$ as found in the 3Pt1Sn/C catalyst causes this particular catalyst to have better durability compared to the commercial Pt/C catalyst in the accelerated stability test.

## Acknowledgements

This work was financially supported by the Korea Gas Corporation, the Brain Korea 21 Project, and the ERC Program of MOST/KOSEF (Grant No. R11-2002-102-00000-0).

## References

[1] T. Iwasita, H. Hoster, A. John-Anaker, W.F. Lin, W. Vielstich, Langmuir 16 (2000) 522.
[2] D.-H. Lim, L. Lu, D.B. Kim, D.-H. Choi, D.-R. Park, H.-I. Lee, J. Nanopart. Res. 10 (2008) 1215.
[3] D.-H. Lim, W.-D. Lee, D.-H. Choi, D.-R. Park, H.-I. Lee, J. Power Sources 185 (2008) 159.
[4] D.-H. Lim, W.-D. Lee, H.-I. Lee, Catal. Surv. Asia 12 (2008) 310.
[5] S. Song, W. Zhou, Z. Liang, R. Cai, G. Sun, Q. Xin, V. Stergiopoulos, P. Tsiakaras, Appl. Catal. B: Environ. 55 (2005) 65.
[6] H.A. Gasteiger, N. Markovic, P.N. Ross Jr., E.J. Cairns, J. Electrochem. Soc. 141 (1994) 1795.
[7] S.-A. Lee, K.-W. Park, B.-K. Kwon, Y.-E. Sung, J. Ind. Eng. Chem. 9 (2002) 63.
[8] C. Kim, H.-H. Kwon, I.K. Song, Y.-E. Sung, W.S. Chung, H.-I. Lee, J. Power Sources 171 (2007) 404.
[9] M. Arenz, V. Stamenkovic, B.B. Blizanac, K.J. Mayrhofer, N.M. Markkovic, P.N. Ross, J. Catal. 232 (2005) 402.
[10] I. Honma, T. Toda, J. Electrochem. Soc. 150 (2003) A1689.
[11] W.S. Cardoso, M.S.P. Francisco, A.M.S. Lucho, Y. Gushiken, Solid State Ionics 167 (2004) 165.
[12] F. Colmati, E. Antolini, E.R. Gonzalez, Appl. Catal. B: Environ. 73 (2007) 106.
[13] E. Peled, T. Duvdevani, A. Ahron, A. Melman, Electrochem. Solid-State Lett. 4 (2001) A38.
[14] D.-H. Lim, D.-H. Choi, W.-D. Lee, D.-R. Park, H.-I. Lee, Electrochem. Solid-State Lett. 10 (2007) B87.
[15] M. Gotz, H. Wendt, Electrochim. Acta 43 (1998) 3637.
[16] A.O. Neto, M.J. Giz, J. Perez, E.A. Ticianelli, E.R. Gonzalez, J. Electrochem. Soc. 149 (2002) A272.
[17] J.-S. Choi, W.-S. Chung, H.-Y. Ha, T.-H. Lim, I.-H. Oh, S.-A. Hong, H.-I. Lee, J. Power Sources 156 (2006) 466.
[18] B. Moreno, E. Chinarro, J.C. Perez, J.R. Jurado, Appl. Catal. B: Environ. 76 (2007) 368.
[19] H.A. Gasteiger, N.M. Markovic, P.N. Ross Jr., J. Phys. Chem. 99 (1995) 8290.
[20] T. Yajima, N. Wakabayashi, H. Uchida, M. Watanabe, Chem. Commun. (2003) 828.
[21] K.-W. Park, Y.-E. Sung, J. Ind. Eng. Chem. 12 (2006) 165.
[22] S. Ball, A. Hodgkinson, G. Hoogers, S. Maniguet, D. Thompsett, B. Wong, Electrochem. Solid-State Lett. 5 (2002) A31.
[23] Y.Y. Tong, H.S. Kim, P.K. Babu, P. Waszczuk, A. Wieckowski, E. Oldfield, J. Am. Chem. Soc. 124 (2002) 468.
[24] W.J. Zhou, B. Zhou, W.Z. Li, Z.H. Zhou, S.Q. Song, G.Q. Sun, Q. Xin, S. Douvartzides, M. Goula, P. Tsiakaras, J. Power Sources 126 (2004) 16.
[25] E.M. Crabb, R. Marshall, D. Thompsett, J. Electrochem. Soc. 147 (2000) 4440.
[26] F. Colmati, E. Antolini, E.R. Gonzalez, Electrochim. Acta 50 (2005) 5496.
[27] D.-Y. Lee, S.-W. Hwang, I.-S. Lee, J. Power Sources 145 (2005) 147.
[28] L. Jiang, G. Sun, S. Sun, J. Liu, S. Tang, H. Li, B. Zhou, Q. Xin, Electrochim. Acta 50 (2005) 5384.
[29] C. Lamy, S. Rousseau, E.M. Belgasir, C. Coutanceau, J.-M. Leger, Electrochim. Acta 49 (2004) 3901.
[30] M. Hoheisel, S. Speller, J. Kuntze, A. Atrei, U. Bardi, W. Heiland, Phys. Rev. B 63 (2001) 245403.
[31] F. Vigier, C. Coutanceau, F. Hahn, E.M. Belgsir, C. Lamy, J. Electroanal. Chem. 563 (2004) 81.
[32] V. Radmilovic, H.A. Gasteiger, P.N. Ross, J. Catal. 154 (1995) 98.
[33] A.K. Shukla, M.K. Ravikumar, A. Roy, S.R. Baraman, D.D. Sarma, A. Arico, V. Antonucci, L. Pino, N. Giordano, J. Electrochem. Soc. 141 (1994) 1517.
[34] V. Radmilovic, T.J. Richardson, S.J. Chen, P.N. Ross Jr., J. Catal. 232 (2005) 199.
[35] D.-H. Lim, W.-D. Lee, D.-H. Choi, H.-H. Kwon, H.-I. Lee, Electrochem. Commun. 10 (2008) 592.
[36] E.V. Spinace, A.O. Neto, M. Linardi, J. Power Sources 129 (2004) 121.
[37] S. Mukerjee, J. McBreen, J. Electrochem. Soc. 146 (1999) 600.
[38] V.I. Kuznetsov, A.S. Belyi, E.N. Yurchenko, M.D. Smolikov, M.T. Protasova, E.V. Zatolokina, V.K. Duplayakin, J. Catal. 99 (1986) 159.
[39] A.K. Shukla, A.S. Arico, K.M.E. Khatib, H. Kim, P.L. Antonucci, V. Antonucci, Appl. Surf. Sci. 137 (1999) 20.
[40] C. Roth, M. Goetz, H. Fuess, J. Appl. Electrochem. 31 (2001) 793.
[41] D.F.A. Kouch, D.A.J. Rand, R. Woods, J. Electroanal. Chem. 70 (1976) 73.
[42] J.R.C. Salgado, E. Antolini, E.R. Gonzalez, J. Power Sources 138 (2004) 56.
[43] N.M. Markovic, H.A. Gasteiger, P.N. Ross Jr., X. Jiang, I. Villegas, M.J. Weaver, Electrochim. Acta 40 (1995) 91.
[44] H. Li, G. Sun, L. Cao, L. Jiang, Q. Xin, Electrochim. Acta 52 (2007) 6622.
[45] R.B. de Lima, V. Paganin, T. Iwasita, W. Vielstich, Electrochim. Acta 49 (2003) 85.
[46] A. Pozio, M. de Francesco, A. Cemmi, F. Cardellini, L. Giorgi, J. Power Source 105 (2002) 13.
[47] M. Ciureanu, H. Wang, J. Electrochem. Soc. 146 (1999) 4031.
[48] L. Dubau, F. Hahn, C. Countaceau, J.-M. Leger, C. Lamy, J. Electroanal. Chem. 554 (2003) 407.
[49] Y. Takasu, T. Fujiwara, Y. Murakami, K. Sasaki, M. Oguri, T. Asaki, W. Sugimoto, J. Electrochem. Soc. 147 (2000) 4421.
[50] A.O. Neto, T.R.R. Vasconcelos, R.W.R.V. da Silva, M. Linardi, E.V. Spinace, J. Appl. Electrochem. 35 (2005) 193.
[51] Y. Morimoto, E.B. Yeager, J. Electroanal. Chem. 441 (1998) 77.
[52] K. Wang, H.A. Gasteiger, N.M. Markovic, P.N. Ross, Electrochim. Acta 41 (1996) 2587.
[53] H. Massong, H. Wang, G. Samjeske, H. Baltruschat, Electrochim. Acta 46 (2000) 701.
[54] F. Zaragoza-Martin, D. Sopena-Escario, E. Morallon, C. Salinas-Martinez de Lecea, J. Power Sources 171 (2007) 302.
[55] J. Zhang, K. Sasaki, E. Sutter, R.R. Adzic, Science 310 (2007) 220.